WCTE 2021
WORLD CONFERENCE ON TIMBER ENGINEERING
SANTIAGO, CHILE | 9 - 12 AUGUST

ANALYTICAL AND NUMERICAL INVESTIGATIONS ON IMPERFECTION-SENSITIVE TIMBER MEMBERS SUBJECTED TO COMBINED BENDING AND AXIAL COMPRESSION

Janusch Töpler[1], Ulrike Kuhlmann[2]

ABSTRACT: The verification of slender timber members at risk of lateral torsional buckling is one of the basic verifications in timber design. However, latest investigations have shown that the design formulas provided in Eurocode 5 for imperfection-sensitive members subjected to combined bending and compression tend to be conservative and more advanced verification methods are needed. Analytical and numerical models are presented that allow for the consideration of the geometrically and materially nonlinear behaviour as well as of the size effect of tensile strength $f_{t,0}$ for N_x-M_y-M_z interaction. These models and calculation results increase the understanding of the main influencing parameters of the load-bearing capacity of imperfection-sensitive timber beams and columns and may be the basis of a revision of the current design formulas provided in EN 1995-1-1.

KEYWORDS: Cross-section verification, stability, lateral torsional buckling, size effect, plasticising

1 INTRODUCTION

Material-efficiency in long-spanning timber constructions is becoming more and more important, also due to currently rapidly increasing material prices. For the design of such slender timber structures (Figure 1), which are typically subjected to a combined loading of bending and axial compression, stability failure is often dominant.
This failure mechanism is characterised by excessive deformations and associated additional internal forces (**geometrically nonlinear behaviour**). In the case of members subjected to bending stresses with additional compressive stresses and/or a lower compressive than bending strength ($f_{c,0} < f_m$), **materially non-linear behaviour** occurs. This appears in the form of a plasticising in the compression zone when the proportionality limit is exceeded at approx. 70 to 80 % of the compressive strength along the grain $f_{c,0}$ [9]. Due to the material scattering, the tensile and bending strengths of wood along the grain are significantly influenced by the stress distribution over the length, height and width of the member, also known as **size effect**.
The presented analytical and numerical models were developed to incorporate these three effects for an investigation of their influence on the load-bearing behaviour of imperfection-sensitive timber beams and columns.

2 STATE OF THE ART

EN 1995-1-1 [5],[7] provides two different verification concepts for the design of slender timber members, where one is the effective length method and the other verification method is based on calculation according to second order theory. The separate verification methods of the equivalent length method for compression and bending (hereafter referred to as k_c- and k_m-method) have been verified by analytical, numerical and experimental investigations [1],[14]. They provide the designing structural engineer with simple and sufficiently accurate design formulas, which however are based on different assumptions for the imperfections. The imperfection assumptions are currently investigated in a DIBt project at the Institute of Structural Design [13].
However, there are only few experimental investigations and no full-scale tests on slender timber members subjected to combined bending and compression prone to lateral torsional buckling known. For the combined effective length method (k_c-k_m-method), a pragmatic linear interaction is used according to EN 1995-1-1 [5],[7]. For a verif-

Figure 1: *Glulam beams subjected to bending and compression due to vertical and horizontal loading*

[1] Janusch Töpler, M.Sc., University of Stuttgart, Institute of Structural Design, Stuttgart, Germany, janusch.toepler@ke.uni-stuttgart.de

[2] Prof. Dr.-Ing. Ulrike Kuhlmann., University of Stuttgart, Institute of Structural Design, Stuttgart, Germany, sekretariat@ke.uni-stuttgart.de

ication on the basis of calculations of second order theory the interaction formulas derived by Buchanan [2] with a quadratic compression component may be used [7]. Hörsting [10] developed an analytical model for the calculation of internal forces according to second order theory. For a realistic representation of the load-bearing behaviour of imperfection-sensitive timber members he incorporated plasticising and the size effect according to Weibull [18]. For relative slenderness ratios $\lambda_{rel,m} \leq 1.15$ a significant increase of the load-bearing capacity up to 30 % due to these two effects can be observed [12].
So far, the influence of plasticising has only been discussed in relation to the resistance [10] and not concerning its effect on the geometrically nonlinear calculation of the internal forces. Further, there are no known experimental studies on imperfection-sensitive timber members at N_x-M_y interaction to validate the theoretical models. This also applies to the volume effect in biaxial bending.

3 ANALYTICAL MODEL

3.1 GENERAL

The model is based on the work of Hörsting [10] and is extended by an approach for the consideration of the materially nonlinear behaviour when calculating internal forces according to second order theory. A brittle tension failure is assumed to be prevailing. The investigated structural system, geometry and coordinate system are shown in Figure 2. The model is implemented in Matlab.

3.2 GEOMETRICAL NONLINEARITY

The known formulas for the calculation of internal forces according to second theory order are used:

$$M_{y,II} = \frac{M_y(1+\alpha_{c,y}\cdot\delta)-N_x e_z}{1-\alpha_{c,y}} \tag{1}$$

$$M_{z,II} = \frac{(-N_x+M_y^2/GI_x)\cdot e_y+M_y e_\vartheta}{1-\alpha_{c,z}-\alpha_m^2} \tag{2}$$

$$\alpha_m = \frac{M_y}{M_{y,crit}} \quad \text{with} \quad M_{y,crit} = \frac{\pi}{L_{m,ef}}\sqrt{GI_x EI_z} \tag{3}$$

$$\alpha_{c,y/z} = \frac{N_x}{N_{crit,y/z}} \quad \text{with} \quad N_{crit,y/z} = -\frac{\pi^2 EI_{y/z}}{L_{c,y/z,ef}^2} \tag{4}$$

where M_y = bending moment around the y-axis (Figure 2), N_x = normal force (tension positive, Figure 2), δ = Dischinger-coefficient taking into account the distribution of M_y, $e_{y/z/\vartheta}$ = sinusoidal imperfections (Figure 3), $I_{x/y/z}$ = moments of inertia (Equations (13) to (16)), E = Young's modulus E_m, G = shear modulus G_{xz}, $L_{c,y/z/m,ef}$ = effective lengths under consideration of bending and normal force. The derivation of the equations is based on following assumptions [10]:

- Isotropic and homogeneous material behaviour,
- prismatic rectangular cross-section,
- flat surfaces remain flat,
- small deformations (sin x = x and cos x = 1),
- change of length may be neglected,
- shear deformations may be neglected,

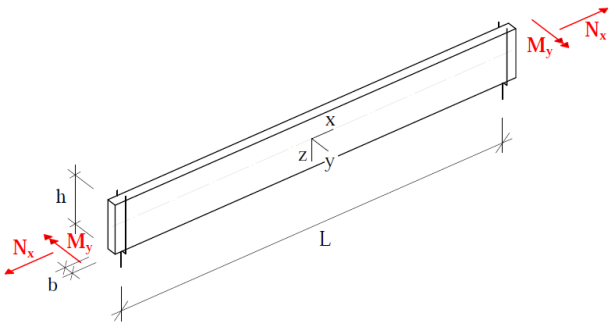

Figure 2: *Structural system, geometry and coordinate system*

- warping resistance may be neglected,
- products of deformations are neglected.

3.3 MATERIAL NONLINEARITY

The idealised stress-strain relationship in Figure 4 is assumed. Exceeding of the bending strength f_m in the tensile zone is chosen as failure criterion.
An exemplary stress distribution across the cross-section under N_x-M_y and N_x-M_y-M_z loading assuming an ideal elasto-plastic material behaviour is shown in Figure 5 and Figure 6. The stress and strain distribution over the cross-section for an over the length constant N_x-M_y-M_z loading when reaching the **load-bearing capacity** is:

$$\varepsilon(y,z) = \kappa_y \cdot \left(z - \frac{h}{2}\right) + \kappa_z \cdot \left(y - \frac{b}{2}\right) + \varepsilon_{t,0} \tag{5}$$

$$\sigma(y,z) = E \cdot \left[\varepsilon(y,z) + \langle -(\varepsilon(y,z) - \varepsilon_{c,0})\rangle\right] \tag{6}$$

where ε = strain in x-direction, σ = stress in x-direction, $\kappa_{y/z}$ = curvatures, b and h = cross-section width and height, $\varepsilon_{t,0} = f_m / E$, $\varepsilon_{c,0} = f_{c,0} / E$, $\langle\ \rangle$ = Macaulay brackets.

When integrating the stresses over the cross-section area, the relation between stress / strain distribution, curvatures $\kappa_{y/z}$ and load-bearing capacities $N_{x,R}$, $M_{y,R}$, $M_{z,R}$ can be determined to:

$$N_{x,R} = \int_{-h/2}^{h/2}\int_{-b/2}^{b/2} \sigma(y,z)\, dy\, dz \tag{7}$$

$$M_{y,R} = \int_{-h/2}^{h/2}\int_{-b/2}^{b/2} z\cdot\sigma(y,z)\, dy\, dz \tag{8}$$

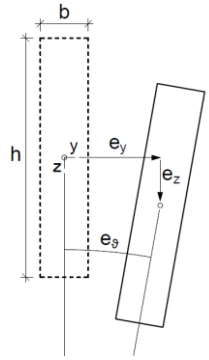

Figure 3: *Ideal and actual position of the cross-section, imperfections at midspan*

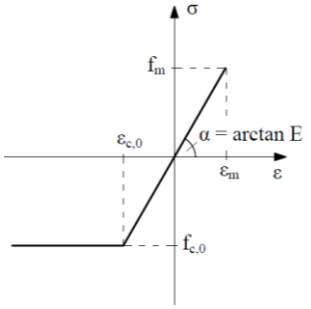

Figure 4: *Assumed stress-strain relationship along the grain*

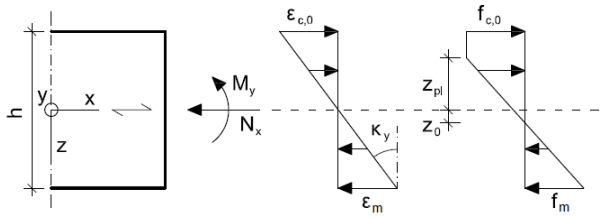

Figure 5: *Stress and strain distribution for N_x-M_y loading when reaching the load-bearing capacity*

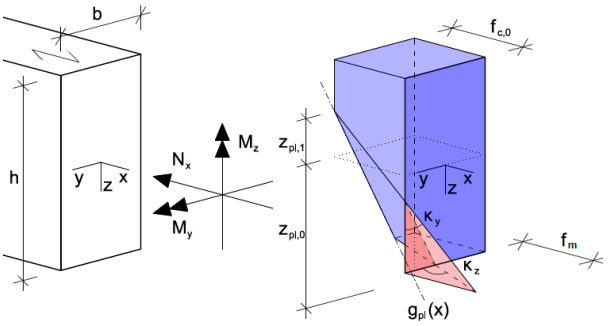

Figure 6: *Stress distribution for N_x-M_y-M_z loading when reaching the load-bearing capacity*

$$M_{z,R} = \int_{-h/2}^{h/2} \int_{-b/2}^{b/2} y \cdot \sigma(y,z)\, dy\, dz \qquad (9)$$

where $N_{x,R}$, $M_{y,R}$, $M_{z,R}$ represent the load-bearing capacities of a cross-section for specific curvatures $\kappa_{y/z}$, maximum strains $\varepsilon_{c,0}$ and $\varepsilon_{t,0}$ and stiffnesses EA, $EI_{y/z}$.

When solving (7) to (9), this results in Equations (10) to (12). By the Macaulay brackets these equations contain 5 different cases, which can be graphically interpreted as different shapes of the plastic region, where g_{pl} represents the plastic regions' lower boundary as shown in Figure 7. $z_{pl,0/1}$ are the z-coordinates of g_{pl} at y = +/- b/2. For a more detailed description see [10]. For the stability of the analytical calculations, when $\kappa_{y/z}$ is close to 0, Equations (10) to (12) can be solved separately for each of the 5 cases in order to avoid the corresponding $\kappa_{y/z}$ being in the denominator. Due to their complexity, these transformations are not shown here.

The load-bearing capacity of a cross-section with h x b = 500 x 100 mm made of glulam GL 24h with

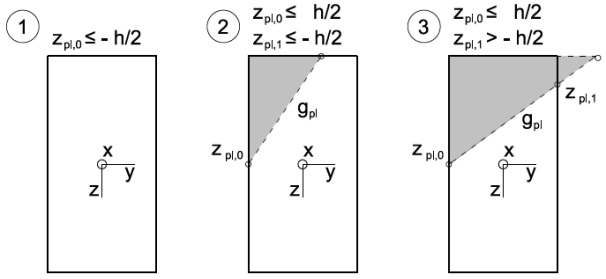

(a) cases 1 to 3

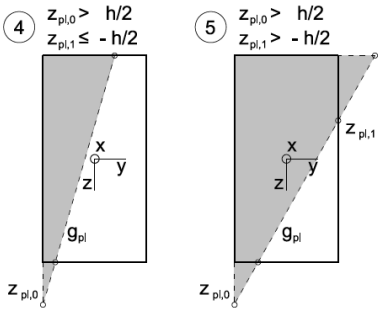

(a) cases 4 and 5

Figure 7: *5 different cases of the shape of the plastic region, where the plasticised region is shaded grey with $z_{pl,0/1}$ as z-coordinates of g_{pl} at y = +/- b/2*

E = 11500 N/mm², $f_{c,0}$ = f_m = 24 N/mm² calculated with Equations (10) to (12) for N_x-M_y loading is displayed in Figure 8 and for N_x-M_y-M_z loading in Figure 9. The Young's modulus does not influence the results. In comparison the load-bearing capacity according to EN 1995-1-1 Eq. (6.19) and (6.20) with k_m = 1.0 is displayed in Figure 8. Thereby, no partial factors, no geometrically nonlinear behaviour nor a size effect are considered. It can be seen that Equations (10) to (12) can be used to determine higher load-bearing capacities for combined compression and bending than according to formulas (6.19) and (6.20) in EC5 [7].

As soon as plasticising occurs, this also reduces the **cross-sectional stiffness**, which should be taken into account when calculating internal forces according to second order theory (Equations (1) to (4)). When assuming ideal elasto-plastic material behaviour (Figure 4), there is no more residual stiffness of the plasticised area if $\varepsilon_{c,0}$ is exceeded. The residual stiffness of the not yet plasticised re-

$$N_{x,R} = EA \cdot \left(\varepsilon_{t,0} - \frac{\kappa_y h}{2} - \frac{\kappa_z b}{2}\right) + \frac{E}{6\kappa_y \kappa_z} \cdot \begin{pmatrix} \langle -(\varepsilon_{t,0} - \varepsilon_{c,0} - h\kappa_y - b\kappa_z)\rangle^3 \\ -\langle -(\varepsilon_{t,0} - \varepsilon_{c,0} - h\kappa_y)\rangle^3 \\ -\langle -(\varepsilon_{t,0} - \varepsilon_{c,0} - b\kappa_z)\rangle^3 \end{pmatrix} \qquad (10)$$

$$M_{y,R} = EI_y\, \kappa_y - \frac{E}{24\kappa_y^2 \kappa_z} \cdot \begin{pmatrix} \langle -(\varepsilon_{t,0} - \varepsilon_{c,0} - h\kappa_y - b\kappa_z)\rangle^3 \cdot (\varepsilon_{t,0} - \varepsilon_{c,0} - h\kappa_y - b\kappa_z) \\ -\langle -(\varepsilon_{t,0} - \varepsilon_{c,0} - h\kappa_y)\rangle^3 \cdot (\varepsilon_{t,0} - \varepsilon_{c,0} - h\kappa_y) \\ -\langle -(\varepsilon_{t,0} - \varepsilon_{c,0} - b\kappa_z)\rangle^3 \cdot (\varepsilon_{t,0} - \varepsilon_{c,0} - 2h\kappa_y - b\kappa_z) \end{pmatrix} \qquad (11)$$

$$M_{z,R} = EI_z\, \kappa_z - \frac{E}{24\kappa_y \kappa_z^2} \cdot \begin{pmatrix} \langle -(\varepsilon_{t,0} - \varepsilon_{c,0} - h\kappa_y - b\kappa_z)\rangle^3 \cdot (\varepsilon_{t,0} - \varepsilon_{c,0} - h\kappa_y - b\kappa_z) \\ -\langle -(\varepsilon_{t,0} - \varepsilon_{c,0} - h\kappa_y)\rangle^3 \cdot (\varepsilon_{t,0} - \varepsilon_{c,0} - h\kappa_y - 2b\kappa_z) \\ -\langle -(\varepsilon_{t,0} - \varepsilon_{c,0} - b\kappa_z)\rangle^3 \cdot (\varepsilon_{t,0} - \varepsilon_{c,0} - b\kappa_z) \end{pmatrix} \qquad (12)$$

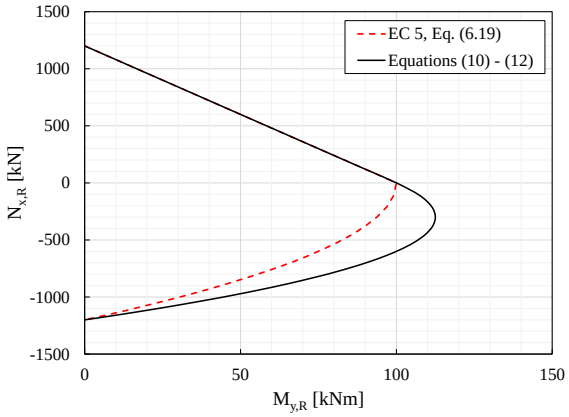

Figure 8: *Load-bearing capacity of a cross-section with h x b = 500 x 100 mm made of GL 24h for N_x-M_y loading according to the analytical model and EN 1995-1-1*

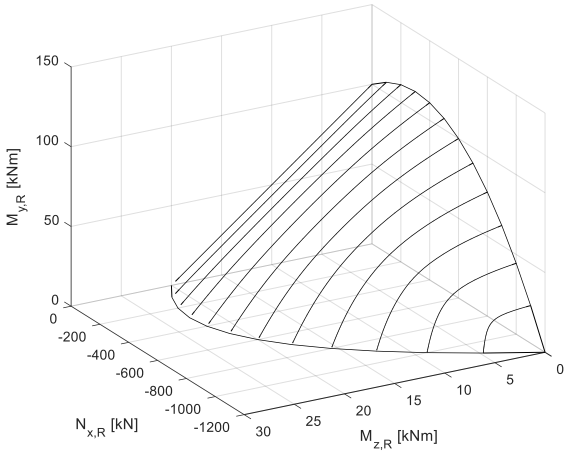

Figure 9: *Load-bearing capacity of a cross-section with h x b = 500 x 100 mm made of GL 24h for N_x-M_y-M_z loading according to the analytical model*

maining polygonal cross-section area (Figure 7) can be determined according to Equations (13) to (16) [16].

$$A = \frac{1}{2} \cdot \sum_{i=1}^{n-1} (y_i \cdot z_{i+1} - y_{i+1} \cdot z_i) \tag{13}$$

$$I_y = \frac{1}{12} \cdot \sum_{i=1}^{n-1} \{(y_i \cdot z_{i+1} - y_{i+1} \cdot z_i) \cdot [(z_i + z_{i+1})^2 - z_i \cdot z_{i+1}]\} \tag{14}$$

$$I_z = \frac{1}{12} \cdot \sum_{i=1}^{n-1} \{(y_i \cdot z_{i+1} - y_{i+1} \cdot z_i) \cdot [(y_i + y_{i+1})^2 - y_i \cdot y_{i+1}]\} \tag{15}$$

$$I_x = \frac{A^4}{4\pi^2 (I_y + I_z)} \tag{16}$$

where n = number of corner points of a polygon, where the first n = 1 and the last n = n coincide, y_i/z_i = y/z-coordinates of the i^{th} corner point.

Equation (16) is the approximation formula for cross-sections free of warping according to St. Venant. For h / b = 5, the results according to this formula are a maximum of 15 % smaller than according to numerical calculations with the DICKQ programme from Dlubal [11]. The largest deviations result for triangular cross-sections with 15 % (case 5 in Figure 7). For approximately rectangular cross-sections the deviations are less than 3 %.

When using the plastic **cross-section stiffness** values according to Equations (13) to (16) for calculations of second order theory (Equations (1) to (4)), it is assumed that the reduced cross-section values apply over the entire length. Thus, conservative cross-section stiffnesses are assumed, which leads to an estimation of the internal forces on the safe side. The calculation of the cross-sectional **load-bearing capacity** according to Equations (10) to (12) is exact for an ideal elasto-plastic material behaviour according to Figure 4.

3.4 SIZE EFFECT

Extensive experimental and theoretical studies on the size effect of the different material strengths of timber have been published, e.g. by [3],[4],[8]. At this point, however, a simplified calculation approach based on the Weibull theory [18] is applied. This approach allows for an extrapolation of the tensile strength $f_{t,0}$ and bending strength f_m to a modified tensile strength $f_{t,0,mod}$ for biaxial bending due to the size effect [10]. A size effect of other material parameters is neglected.
According to Weibull theory, the failure probability S for constant tension can be determined as a function of the acting stress σ according to Equation (17) [10]. For constant uniaxial bending S can be determined according to Equation (18) [10]:

$$S(\sigma) = 1 - \exp\left(-\frac{L}{L_0} \cdot \frac{h}{h_0} \cdot \frac{b}{b_0} \cdot \left(\frac{\sigma}{\sigma_0}\right)^m\right) \tag{17}$$

$$S(\sigma) = 1 - \exp\left(-\frac{L}{L_0} \cdot \frac{h}{2h_0} \cdot \frac{b}{b_0} \cdot \frac{1}{m+1} \cdot \left(\frac{\sigma}{\sigma_0}\right)^m\right) \tag{18}$$

where S = failure probability, σ = stress, L, h, b = member dimensions, L_0, h_0, b_0 = reference member dimensions for which material constants σ_0 and m have been determined.

By substituting $\sigma = f_{t,0,k}$ into Equation (17), $\sigma = f_{m,k}$ into Equation (18) and equating the two resulting equations ($S(\sigma = f_{t,0,k}) = S(\sigma = f_{m,k}) = 0.05$), the material constants σ_0 and m can be determined. For GL 24h with $f_{t,0,k}$ = 19.2 N/mm² and $f_{m,k}$ = 24.0 N/mm² the following values result [6]:

$$\text{GL 24h: } \sigma_0 = 23.19 \frac{N}{mm^2} \quad \text{and} \quad m = 15.73 \tag{19}$$

For biaxial bending with any M_y to M_z ratio, the failure probability S(σ) can be determined according to Equation (21) [10].
Substituting $\sigma = \varepsilon_m E$ into Equation (18) and equating the resulting equation with Equation (21) yields Equation (22). This equation can be used to determine the ultimate strain $\varepsilon_{t,0}$ for biaxial bending under consideration of the size effect according to Weibull theory.
The modified tensile strength $f_{t,0,mod}$ due to the size effect in biaxial bending can then be determined to:

$$f_{t,0,mod} = \varepsilon_{t,0} \cdot E \tag{20}$$

$$S(\sigma) = 1 - \exp\left[\frac{L}{L_0}\cdot\frac{h}{h_0}\cdot\frac{b}{b_0}\cdot\left(\frac{E}{\sigma_0}\right)^m\cdot\frac{\varepsilon_{t,0}^{m+2}-\langle\varepsilon_{t,0}-h\cdot\kappa_y\rangle^{m+2}-\langle\varepsilon_{t,0}-b\cdot\kappa_z\rangle^{m+2}+\langle\varepsilon_{t,0}-h\cdot\kappa_y-b\cdot\kappa_z\rangle^{m+2}}{\kappa_y\cdot\kappa_z\cdot(m+1)\cdot(m+2)}\right] \quad (21)$$

$$\varepsilon_m = \left(2\cdot\frac{L}{L_0}\cdot\frac{h}{h_0}\cdot\frac{b}{b_0}\cdot\frac{\varepsilon_{t,0}^{m+2}-\langle\varepsilon_{t,0}-h\cdot\kappa_y\rangle^{m+2}-\langle\varepsilon_{t,0}-b\cdot\kappa_z\rangle^{m+2}+\langle\varepsilon_{t,0}-h\cdot\kappa_y-b\cdot\kappa_z\rangle^{m+2}}{\kappa_y\cdot\kappa_z\cdot(m+2)}\right)^{\frac{1}{m}} \quad (22)$$

where $\varepsilon_{t,0}$ is the ultimate strain depending on the size effect, curvatures $\kappa_{y/z}$ and material constants $\varepsilon_m = f_m/E$, σ_0 and m.

It should be noted that here, too, on the safe side, a constant loading of the cross-section over the entire length is assumed. If the actual bending moment distributions $M_{y,II}$ and $M_{z,II}$ over the length L are taken into account a higher modified tensile strength $f_{t,0,mod}$ can be determined due to the size effect. Further on, it is assumed for the derivation of Equation (22):

- Zipper effect, no load redistribution is possible,
- distribution of tensile strength $f_{t,0}$ can be mapped by a Weibull distribution (assumption of a lognormal distribution leads to a significant overestimation of the size effect for smaller loaded member volumes),
- failure probabilities within a member are independent of each other,
- no distinction between the size effect for length, height and width.

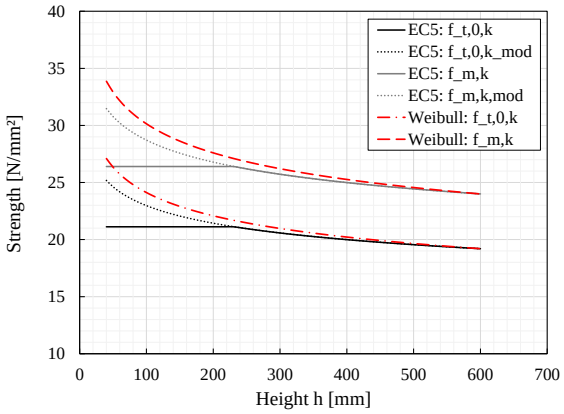

Figure 10: *Influence of the size effect of the tensile and bending strength according to EN 1995-1-1 [7] and Equation (17) and (18); for "_mod" $k_h \leq 1.1$ from [7] is neglected*

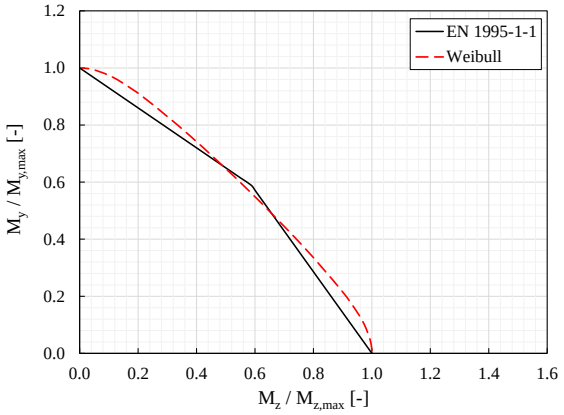

Figure 11: *Influence of the size effect of the biaxial bending strength according to EN 1995-1-1 [7] and Equation (22)*

In Figure 10 and Figure 11 the size effect, determined according to the Weibull theory with Equations (17), (18) and (22), is compared with calculation results according to EN 1995-1-1 [7] Equations (3.2), (6.19), (6.20). For GL 24h k_m = 0.7, $f_{t,0}$ = 24 N/mm² and $f_{c,0}$ = 24,0 N/mm² are chosen [6],[7]. For the curves „_mod" in Figure 10 the limit criterion $k_h \leq 1.1$ from EN 1995-1-1 [7] Equation (3.2) is neglected. Figure 10 shows the tensile strength $f_{t,0,k}$ and bending strength $f_{m,k}$ in consideration of the size effect as a function of the member height h. Figure 11 displays the normalised load-bearing capacity of a cross-section subjected only to biaxial bending. Overall, there is a good agreement between the presented calculation approach according to Weibull theory and the design formulas according to EN 1995-1-1 [7], whereby slightly larger load-bearing capacities can generally be determined using Weibull theory.

A validation of the analytical model to account for the size effect of the tensile strength $f_{t,0}$ for biaxial bending based on experimental investigations is still pending.

3.5 CALCULATION PROCEDURE

Solving a combination of Equations (1) to (4) with (10) to (12), (13) to (16) and (22) is not possible with the available solvers in Matlab. Therefore, a separate solution using graphical methods is chosen.
With input values for material parameters, the cross-section dimensions and N_x the $M_{y,R}$ - $M_{z,R}$ curve 1 of the cross-section resistance (Equation (10) to (12)) including the size effect (Equation (22)) can be calculated iteratively (Figure 12). Next, curve 2 of $M_{y,II}$ can be calculated depending on $M_{z,II}$ (Equations (1) to (4)) and plotted in Figure 12. Then, the intersection of both curves can be deter-

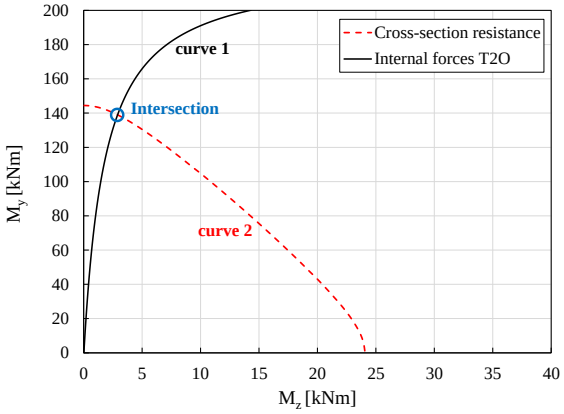

Figure 12: *M_y-M_z interaction of cross-section resistance according to Equations (10) to (12) and (22) for a given N_x and internal forces $M_{y,II}$ and $M_{z,II}$ according to (1) to (4)*

mined, which gives the sought load-bearing capacity $M_{y,R}$ and $M_{z,R}$. In Figure 12 the $M_{y,R}$ - $M_{z,R}$ and $M_{y,II}$ - $M_{z,II}$ interaction curves (Equations (1) to (4), (10) to (12) and (22)) for a cross-section with L x h x b = 3600 x 600 x 100 mm³, with E = 11500 N/mm², G = 650 N/mm², $f_{c,0} = f_{t,0} = f_m$ = 24 N/mm², e_y =L/1000, e_z = 0, e_ϑ = 0.05xb/h and structural system according to Figure 2 with N_x = - 10 kN are displayed.
Based on the curvatures κ_y and κ_z resulting from $M_{y,R}$ and $M_{z,R}$ at the intersection, the cross-section stiffnesses (Equation (13) to (16)) can be updated, the $M_{y,II}$ - $M_{z,II}$ curve 2 recalculated and a new intersection with the $M_{y,R}$ - $M_{z,R}$ curve 1 determined.
The last step is repeated until, $M_{y,II}$ and $M_{z,II}$ converge and an abort criterion is reached.

4 NUMERICAL MODEL

4.1 GENERAL

The numerical calculations are performed with a FE-model in Abaqus/CAE 2018. A text-based input is chosen.

4.2 FE-MODEL

Based on planned experiments, prismatic glulam beams with L x h x b = 10000 x 500 x 100 mm³ as the initial geometry are investigated. Boundary conditions and loading are applied according to Figure 2. For a combined loading of compression and bending, the normal force is applied in a first step. In a second step the bending moment is applied and increased, until a failure criterion is reached. Special care has to be taken to avoid restraining effects and stress concentrations at the fork bearings. Sinusoidal imperfections e_y, e_z, e_ϑ (Figure 3) are applied directly via the node coordinates in the text-based input.
For the modelling, 20-node quadratic brick elements with reduced integration (C3D20R) and a mesh fineness of 100 elements in length, 10 in height and 8 in width are chosen. The discretisation is checked in the verification described in Chapter 4.3.
Orthotropic material behaviour is assumed. As failure criterion for tension parallel to the grain, a brittle failure is chosen, when the tensile strength $f_{t,0}$ is exceeded. For compression parallel to the grain, a bilinear stress-strain relation analogous to Figure 4 is used with a minimum residual slope after exceeding $\varepsilon_{c,0}$ to ensure numerical stability.

4.3 VERIFICATION AND VALIDATION

The verification und validation of the numerical model is carried out according to prEN 1993-1-14 [17].

The **verification** ensures a correct implementation of the FE-model. First, an evaluation of the decisive system response quantities (SRQs) due to **engineering judgement** is carried out. Figure 14 shows an example of the displacements of a beam with a constant bending moment M_y according to Finite Element calculations. Stresses, strains and displacements agree well with expected values and simple hand calculations.

This is followed by a check of the **discretisation** (mesh fineness). From 50 elements in length and 6 each in width and height, there is a good agreement of the numerical results with analytical results calculated according to second order theory. For increasing the accuracy of the numerical calculations, a mesh fineness of 100 elements in length, 10 in height and 8 in width is chosen (Figure 14).

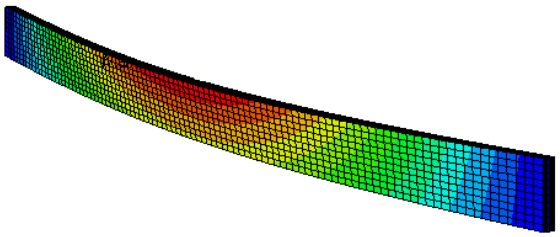

Figure 14: *Numerically derived deformations U2 in y-direction when reaching the load-bearing capacity of the cross-section for a structural system with loading according to Figure 2*

In the last step of verification, a **sensitivity study** is carried out, in which imperfections, material parameters and the type of loading are varied. The influence of the slenderness is evaluated in Chapter 5.
The differences of the SRQ's in calculations with an isotropic or an orthotropic material model are smaller than 1 %. Since the calculation time does not differ significantly, the orthotropic material model is used.
With a concentrated load in z-direction at midspan, there are greater differences between numerical and analytical calculation results than with a constant bending moment M_y. This is due to the fact that the formulas for the calculation of internal forces and deformations according to second order theory (Equations (1) to (4)) were derived for a constant bending moment and do not take into account shear deformations due to shear forces.
For smaller imperfections the relative differences between analytical and numerical results become smaller. The determined elastic load-bearing capacities M_y deviate from each other by a maximum of 1.5 % (numerical results always larger than analytical ones). Numerically larger displacements in the z-direction (34 %) coupled with smaller displacements in the y-direction (35 %) result, when reaching the load-bearing capacity (Figure 13). As a result of the torsion of the cross-section about the x-axis, the effective bending stiffness about the global y-axis is reduced. Since the torsion increases non-linearly with in-

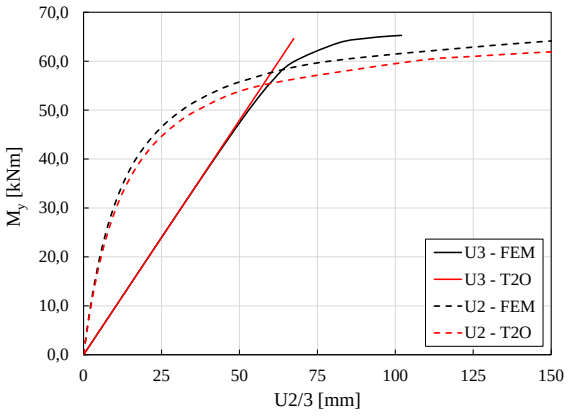

Figure 13: *Deformations in y- (U2) and z-direction (U3) at midspan of a glulam beam (Figure 2) subjected to a constant bending moment M_y*

creasing M_y, the displacement in the z-direction consequently also increases non-linearly, which is not represented by the analytical Equations (1) to (4). On the other hand, as a result of the simplifications, the horizontal stiffness is underestimated in analytical calculations compared to numerical calculations. The latter effect seems to prevail, which means that analytically determined elastic load-bearing capacities are usually on the safe side compared to numerically determined ones.
Thus, the numerical model is verified.

In **validation**, by comparing numerical calculation results with experimental investigations or other known exact solutions (benchmark cases), it can be shown that a model correctly (or approximately accurately) represents the desired physical behaviour.
Here, only a comparison with analytical calculation results is carried out (see Chapter 5).

5 RESULTS

5.1 GENERAL

The calculations are carried out for GL 24h with material parameters according to Table 1.

Table 1: *Used material parameters for GL 24h [6],[15]*

E_x	11,500	N/mm²
E_y	300	N/mm²
E_z	300	N/mm²
G_{xy}	650	N/mm²
G_{xz}	650	N/mm²
G_{yz}	65	N/mm²
ν_{xy}	0.4096	
ν_{xz}	0.5542	
ν_{yz}	0.5993	
$f_{c,0}$	24.0	N/mm²
f_m	24.0	N/mm²
$f_{t,0}$	19.2	N/mm²

No partial factors are taken into account. The values according to Equation (19) are used as material constants m and σ_0 for the Weibull theory. For consistency, f_m is chosen as the tensile strength for numerical calculations. Sinusoidal imperfections e_y = L/1000, e_z = 0 and e_ϑ = 0.05 b/h with a maximum at midspan are chosen (Figure 3). The assumed structural system is displayed in Figure 2. In the calculations, the relative slenderness $\lambda_{rel,m}$ (by means of the length L) and the magnitude of the normal force N_x are varied.

5.2 GEOMETRICAL NONLINEARITY

The calculation results of the load-bearing capacities according to Equations (1) to (4) and linear stress interaction (see Equation (23), elastic calculations of second order theory) are compared here with results of Finite Element calculations with purely elastic material behaviour. Exceeding the compressive strength parallel to the grain $f_{c,0}$ is chosen as failure criterion.

$$\frac{-N_x}{A\, f_{c,0}} + \frac{M_{y,II}}{W_y\, f_{c,0}} + \frac{M_{z,II}}{W_z\, f_{c,0}} = 1 \tag{23}$$

In Figure 15 the load-bearing capacity M_y is shown depending on the slenderness. The dotted line marks the maximum bending moment capacity $M_{y,m} = W_y\, f_m$. Figure 16 shows the N_x-M_y interaction diagram for different relative slendernesses. It can be seen that the analytically (Analytic) and numerically (FEM) calculated elastic load-bearing capacities are almost identical. Whereas the numerically determined ones tend to be smaller for small slendernesses and larger for large slendernesses.

5.3 MATERIAL NONLINEARITY

The calculation results of the load-bearing capacities according to Equations (1) to (4), (10) to (12), (13) to (16) (calculations of second order theory combined with reduced plastic cross-section stiffnesses and elasto-plastic cross-section resistance) are compared with results of Finite Element calculations with elasto-plastic material behaviour. Additionally the load-bearing capacity according to Equation (24) from EN 1995-1-1 [7] is determined.

$$\left(\frac{N_x}{A\, f_{c,0}}\right)^2 + \frac{M_{y,II}}{W_y\, f_m} + \frac{M_{z,II}}{W_z\, f_m} = 1 \tag{24}$$

In Figure 17 the load-bearing capacity M_y is shown depending on the slenderness for elasto-plastic material behaviour. The dotted line marks the maximum bending moment capacity $M_{y,m} = W_y\, f_m$. As Equation (24) from

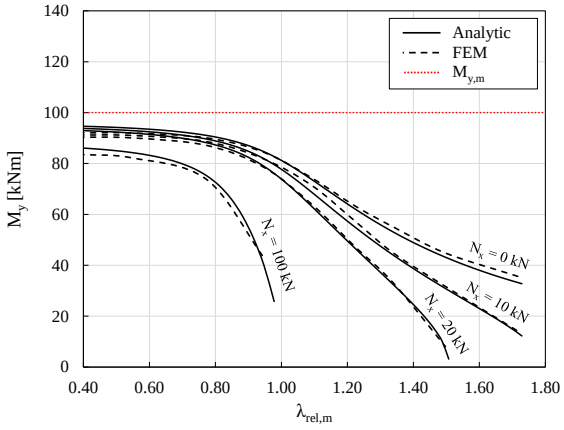

Figure 15: *Load-bearing capacity M_y for different compression forces N_x depending on the relative slenderness $\lambda_{rel,m}$ for linear elastic material behaviour*

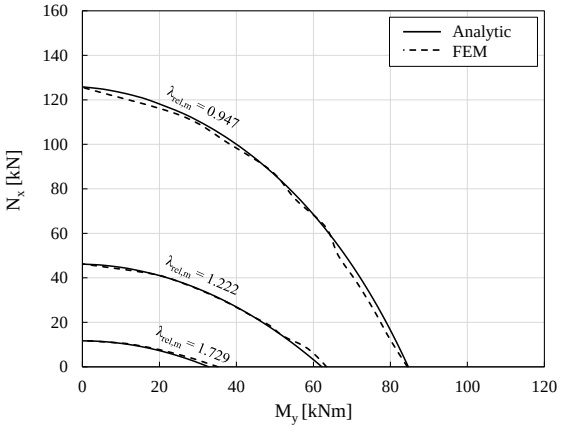

Figure 16: *Interaction diagram of the N_x-M_y load-bearing capacity for different relative slendernesses $\lambda_{rel,m}$ for linear elastic material behaviour*

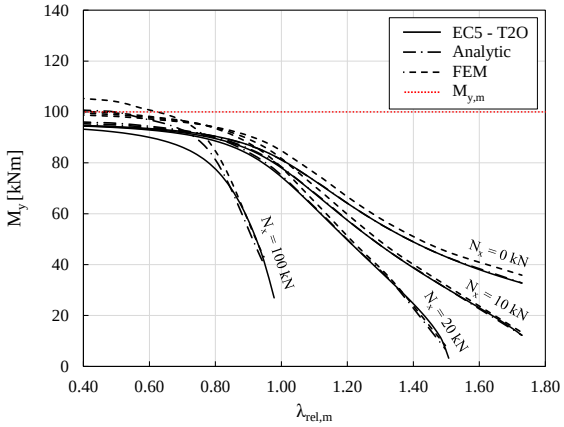

Figure 17: *Load-bearing capacity M_y for different compression forces N_x depending on the relative slenderness $\lambda_{rel,m}$ for elasto-plastic material behaviour*

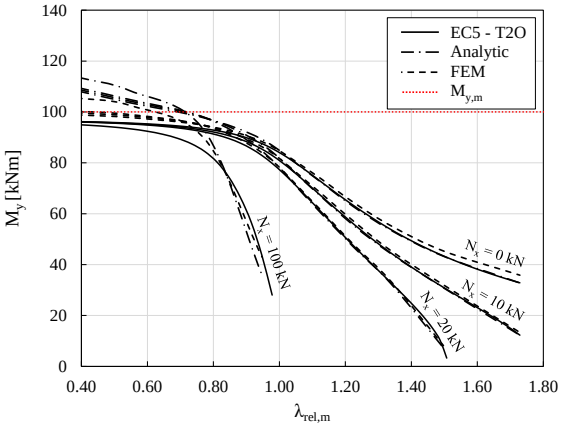

Figure 18: *Load-bearing capacity M_y for different compression forces N_x depending on the relative slenderness $\lambda_{rel,m}$ for elasto-plastic material behaviour with the size effect of $f_{t,0}$*

EN 1995-1-1 [7] does not fully account for the positive influence of a compression force N_x, for stocky beams up to 13 % larger load-bearing capacities can be determined using numerical methods and up to 8 % larger ones using analytical methods (Figure 17). For $\lambda_{rel,m} \geq 1.0$, the results of the different calculation methods are very similar.

5.4 SIZE EFFECT

The calculation results of the load-bearing capacities according to Equations (1) to (4), (10) to (12), (13) to (16) and (22) (calculations of second order theory combined with reduced plastic cross-section stiffnesses, a modified tensile strength $f_{t,0,mod}$ due to the size effect and elasto-plastic cross-section resistance) are compared with results of Finite Element calculations with elasto-plastic material behaviour. Additionally, the load-bearing capacities according to Equations (25) and (26) from EN 1995-1-1 [7] with $k_m = 0.7$ are determined.

$$\left(\frac{N_x}{A\, f_{c,0}}\right)^2 + k_m \frac{M_{y,II}}{W_y\, f_m} + \frac{M_{z,II}}{W_z\, f_m} = 1 \qquad (25)$$

$$\left(\frac{N_x}{A\, f_{c,0}}\right)^2 + \frac{M_{y,II}}{W_y\, f_m} + k_m \frac{M_{z,II}}{W_z\, f_m} = 1 \qquad (26)$$

In Figure 18 the load-bearing capacity M_y is shown depending on the slenderness for elasto-plastic material behaviour including the size effect of $f_{t,0}$. The dotted line marks the maximum bending moment capacity $M_{y,m} = W_y\, f_m$. Additionally to the positive influence of a compression force N_x combined with plasticising (see Chapter 5.3), a positive influence of the size effect of $f_{t,0}$ occurs for $\lambda_{rel,m} \leq 1.0$. Compared to results from Equations (25) and (26) about 10 % larger load-bearing capacities can be determined for stocky beams using numerical methods and about 20 % using analytical methods, whereas the numerical methods do not take the size effect into account.

6 CONCLUSIONS AND OUTLOOK

The paper presents an analytical and a numerical model for the calculation of imperfection-sensitive timber members subjected to combined bending and axial compression, which take into account the geometrically and materially nonlinear behaviour and the size effect of the tensile strength $f_{t,0}$. For the analytical model the considerations of Hörsting [10] are extended to consider the effect of plasticising for the cross-section stiffnesses, in order to fully account for the influence of plasticising. The models show good agreement with known calculation approaches [7] and allow for a separate investigation of the influencing parameters.

Below a relative slenderness $\lambda_{rel,m}$ of 1.0, a significant influence of the size effect and plasticising can be observed using the models. This leads to an increase of the load-bearing capacity of up to 20 % compared to calculations according to EN 1995-1-1 [7].

Future research will focus on the improvement of the convergence of both methods and the implementation of the size effect in the numerical model. To validate the models, full scale experimental tests will be carried out on slender glulam beams under combined bending and compression at the University of Stuttgart.

Finally, based on the experimental results, an improved design concept for slender timber beams and columns will be developed by means of numerical and analytical investigations, which will allow for a better utilisation of existing load-bearing capacity reserves.

ACKNOWLEDGEMENT

Part of this research work (21285 N) is coordinated by the International Association for Technical Issues related to Wood (iVTH e. V.), supported in the program of "Industriellen Gemeinschaftsforschung (IGF)" and financed by the German Federation of Industrial Research Association (AiF).
Partially supported by the Deutsche Forschungsgemeinschaft (DFG, German Research Foundation) under Germany´s Excellence Strategy – EXC 2120/1 – 390831618".

REFERENCES

[1] Blaß, H. J.: Design of timber columns. In: International council for building research studies and documentation - working commission W18A - timber structures (CIB-W18A/20-2-2), Dublin, 1987.

[2] Buchanan, A. H.: Strength model and design methods for bending and axial load interaction in timber members. University of British Columbia, Dissertation, 1984.

[3] Burger, N.: Einfluss der Holzabmessungen auf die Zugfestigkeit von Schnittholz unter Zugbeanspruchung in Faserrichtung. Ludwig Maximilian University Munich, Dissertation, 1998.

[4] Denzler, J. K.: Modellierung des Größeneffektes bei biegebeanspruchtem Fichtenschnittholz. Technical University of Munich, Dissertation, 2007.

[5] DIN EN 1995-1-1/NA: National Annex – Nationally determined parameters – Eurocode 5: Design of timber structures – Part 1-1: General – Common rules and rules for buildings. German Institute for Standardization (DIN), Berlin, 2013.

[6] DIN EN 14080: Holzbauwerke – Brettschichtholz und Balkenschichtholz – Anforderungen. German Institute for Standardization (DIN), Berlin, 2013.

[7] EN 1995-1-1: Eurocode 5: Design of timber structures – Part 1-1: General – Common rules and rules for buildings. European Committee for Standardization (CEN), Brussels, 2004.

[8] Frese, M.: Computergestützte Verfahren zur pragmatischen Beurteilung der Tragwiderstände von Brettschichtholz: Zusammenfassung exemplarischer Simulationsstudien. Karlsruhe Institute of Technology, Habilitation, 2016.

[9] Grosse, M.: Zur numerischen Simulation des physikalisch nichtlinearen Kurzzeittragverhaltens von Nadelholz am Beispiel von Holz-Beton-Verbundkonstruktionen. Bauhaus University Weimar, Dissertation, 2005.

[10] Hörsting, O.-P.: Zum Tragverhalten druck- und biegebeanspruchter Holzbauteile. Technical University of Braunschweig, Dissertation, 2008.

[11] Ingenieur-Software Dlubal GmbH: Programm DICKQ - Querschnittswerte und Bemessung von dickwandigen Querschnitten. Tiefenbach, 2007.

[12] Kuhlmann, U.; Köppel, N.; Töpler, J.: Investigation of lateral torsional buckling of timber beams subjected to bending and axial compression. In: 25th International Wood Construction Conference, IHF 2019, Innsbruck, 2019.

[13] Kuhlmann, U.; Töpler, J.: Imperfections of Slender Glulam Beams. In: Proceedings of the 8th meeting of the International Network on Timber Engineering Research (INTER/54-12-3), online, 2021.

[14] Larsen, H. J.: Laterally loaded timber columns, Tests and theory. In: International council for building research studies and documentation - working commission W18A - timber structures (CIB-W18A/8-15-1), Brussels, 1977.

[15] Neuhaus, F.-H.: Elastizitätszahlen von Fichtenholz in Abhängigkeit von der Holzfeuchtigkeit. Ruhr University Bochum, Dissertation, 1981.

[16] Petersen, C.: Statik und Stabilität der Baukonstruktionen. Friedr. Vieweg & Sohn, 1982.

[17] prEN 1993-1-14 (draft version): Eurocode 3: Design of steel structures – Part 1-14: Design assisted by finite element analysis. CEN/TC 250/SC 3/WG 22 N 32, 14 April 2021.

[18] Weibull, W.: A statistical theory of the strength of materials. Generalstabens litografiska anstalts förlag, 1939.